This is a non-peer reviewed preprint submitted to Atmospheric Pollution Research, Elsevier.

Highlights

Machine-Learning Approaches for Assessing Aerosol Optical Depth (AOD) in Ghana, West Africa

Jesse Gilbert, Jeffrey N. A. Aryee, Mary Jessie Adjei

- MODIS exhibits exceptional performance in retrieving AOD values throughout Ghana.
- The research contributes a comprehensive sixteen-year assessment (2003-2019) of AOD at a 3 km resolution, obtained from MODIS Aqua and Terra satellites.
- The examination of MODIS Aqua and Terra AOD retrievals unveiled an overall lower aerosol burden over Ghana, marked by mean AOD values hovering around 0.35.
- The findings indicate that the southwestern part of the country displays elevated aerosol levels compared to other major cities.
- All machine learning models developed in the study exhibited an acceptable level of accuracy.

Machine-Learning Approaches for Assessing Aerosol Optical Depth (AOD) in Ghana, West Africa

Jesse Gilbert[a], Jeffrey N. A. Aryee[a,*], Mary Jessie Adjei[a]

[a]*Department of Meteorology and Climate Science, Kwame Nkrumah University of Science and Technology, Kumasi, Ghana*

Abstract

In the field of environmental health, assessing air pollution exposure has historically posed challenges, primarily due to sparse ground observation networks. To overcome this limitation, satellite remote sensing of aerosols provides a valuable tool for monitoring air quality and estimating particulate matter concentration (PM) at the surface. In this study, we employ two predictive models to estimate Aerosol Optical Depth (AOD) levels over Ghana and selected localities from January 2003 to December 2019. Our investigation focuses on evaluating the capabilities of multiple linear regression (MLR) and artificial neural network (ANN) models in predicting AOD levels. Additionally, we introduce a novel approach to constructing the MLR model by leveraging the ANN architecture. These models utilize meteorological variables as input, to facilitate accurate predictions. Despite Ghana's alarming air pollution health ranking and its substantial role in mortality, routine monitoring remains sparse. This research contributes a comprehensive sixteen-year assessment (2003-2019) of AOD at a 3 km resolution, obtained from MODIS Aqua and Terra satellites. The findings indicate that the southwestern part of the country displays elevated aerosol levels compared to other major cities. This phenomenon can be attributed to biogenic emissions, given the region's dense vegetation. Additionally, many small cities within this area are recognized as hotspots for surface mining operations, potentially contributing to increased local dust loadings in the atmosphere. Notably, the MLR model, implemented using the ANN model structure, outperformed the other utilized models. This endeavor aims to unravel the spatiotemporal distribution patterns of aerosols across Ghana, and its major urban hubs.

Keywords: Aerosols, Machine Learning, ANN, MLR, MODIS, Ghana

*Corresponding author

Email address: jeff.jay8845@gmail.com (Jeffrey N. A. Aryee)

1. Introduction

Aerosols are airborne particles suspended in the atmosphere, encompassing various compositions and sizes (Kondratyev et al., 2006; Putaud et al., 2010b). These particles emerge from two primary sources: direct emission of primary particulate matter (PM) and secondary particle formation from gaseous precursors. Black carbon (BC), primary biological aerosol particles (PBAPs), sea salt spray, and, mineral dust are some examples of primary aerosols. On the contrary, secondary aerosols arise from processes of sulfate, nitrate, and ammonium formation (Boucher et al., 2013). Aerosols directly influence the atmosphere's energy balance through radiation scattering and absorption (Yu et al., 2006). Furthermore, they act as nuclei for cloud formation (Lohmann and Feichter, 2005), and indirectly impact atmospheric heat by absorbing radiation, contributing to reduced low cloud cover (Johnson et al., 2004). Consequently, aerosols impact the earth's hydrological cycle (Creamean et al., 2013) and, to a considerable extent, food security (Misra, 2014). Fine PM with diameters below 2.5 μm ($PM_{2.5}$) have been linked to negative health outcomes, such as immediate to chronic effects (WHO, 2013). These include aggravated respiratory symptoms (Kato, 2018; Prieto-Parra et al., 2017; Zeng et al., 2016), worsened asthma (Jung et al., 2017; Williams et al., 2019), heightened cardiovascular diseases (Dabass et al., 2018; Vidale and Campana, 2018), diminished lung function (Thaller et al. (2008)), and increased premature mortality linked to heart or lung conditions (Apte et al., 2015; David et al., 2019). The surge in vehicle numbers and land use transformations, largely driven by rapid urban growth in Ghana's major cities (Ministry of Transport, 2016), has led to escalating $PM_{2.5}$ concentrations. These concentrations are significantly affected by local traffic emissions, land use practices like bush burning, and industrial discharges. Rapid and precise assessment of the spatiotemporal distribution of $PM_{2.5}$ (SIERRA-VARGAS and Teran, 2012; Cai et al., 2017) at a finer resolution can enhance the accuracy of health outcome studies related to PM2.5 (Williams et al., 2019), especially when conducted on a local spatial scale. However, $PM_{2.5}$ ground monitoring stations are usually limitedly distributed worldwide, especially for developing countries such as Ghana and its neighbors. This may be a result of resource constraints because establishing and maintaining a network of monitoring stations requires financial investment for equipment, infrastructure, and personnel, which may be challenging for countries with limited budgets. Furthermore, the spatio-temporal variation of $PM_{2.5}$ is complex, influenced by a combination of factors, including local emissions from various sources, meteorological influences, topography, and seasonal patterns such as the movement of the trade winds over Ghana. Long-range transport from diverse geographical

locations and chemical transformations further contribute to this complexity. Without continuous monitoring of $PM_{2.5}$, our ability to rapidly assess, model, and forecast $PM_{2.5}$ levels for Ghana, particularly over the major cities, is severely limited. As an alternative, satellite retrievals are used since they have a wider capture and provide information in most instances even for remote and inaccessible locations. The most relevant satellite-derived parameter for assessing $PM_{2.5}$ concentration levels is Aerosol Optical Depth (AOD) (Wu et al., 2016; Mhawish et al., 2017; Shen et al., 2018; Wei et al., 2019). AOD measures the drop in light intensity caused by aerosol scattering and absorption throughout the atmospheric column (Lee et al., 2011). This metric directly reflects the extent of aerosol presence, providing valuable insights into the overall concentration of optically active particles within each geographical location (Dandou et al., 2002). In the domain of satellite-based aerosol retrievals, AOD datasets are predominantly sourced from two key satellite observations: the Moderate Resolution Imaging Spectroradiometer (MODIS) (Kanabkaew, 2013; Hu et al., 2013; Xu et al., 2016), and the Terra Multi-angle Imaging SpectroRadiometer (MISR) (Liu et al., 2007; Kahn and Gaitley, 2015). MODIS stands out, utilizing Aqua and Terra satellites. Its widespread adoption is owed to its impressive characteristics: a wide swath width covering 2330 kilometers and near-global coverage every 1 to 2 days (Fosu-Amankwah et al., 2021). MODIS aerosol retrievals rely on three main algorithms: Dark Target (DT), Deep Blue (DB), and the combined Dark Target and Deep Blue (DTB) algorithms. Further discussion on these algorithms is provided in Section 2.2.1. This present study utilized the DTB product, based on the DT and DB algorithm. AOD has consistently demonstrated strong correlations with PM measurements (Engel-Cox et al., 2004; Chu et al., 2003; Gupta et al., 2006). Conventional modeling approaches have predominantly relied on chemical transport models (CTMs) and land-use regression (LUR) models, for modeling $PM_{2.5}$ levels while incorporating AOD as a key predictor (Kloog et al., 2012; Geng et al., 2015). Nevertheless, it is worth noting that Land Use Regression models (LURs) have inherent limitations in capturing temporal fluctuations, while Chemical Transport Models (CTMs) may exhibit discrepancies when employed in isolation (Danesh Yazdi et al., 2020). Various statistical methods, spanning from simple univariate regression to complex non-linear models have been developed for the estimation of PM (Danesh Yazdi et al., 2020; Lee et al., 2011; Taheri Shahraiyni and Sodoudi, 2016; Li, 2020; Nabavi et al., 2019). Machine learning (ML) methods have gained popularity in the study of aerosol dynamics and air quality forecasts (Bai et al., 2019; Xiao et al., 2020; Nabavi et al., 2019; Danesh Yazdi et al., 2020). These techniques offer enhanced accuracy and flexibility while requiring smaller datasets compared to traditional models. This shift in approach highlights the need for further research to explore the

potential of ML in advancing our understanding of aerosol dynamics and improving air quality predictions. The application of advanced algorithms enables non-parametric exploration of the intricate relationship between predictor variables and measured pollutant concentrations (Di et al., 2016; Taghavi-Shahri et al., 2020). The current investigation focuses on understanding aerosol dynamics in Ghana, a nation experiencing enhanced population growth and economic expansion (Abokyi et al., 2019). Geographically situated in West Africa, Ghana is influenced by two major trade winds, especially the northwesterly winds carrying Saharan dust. This unique positioning exposes the region to diverse aerosol types and concentrations throughout the year. Agriculture, particularly among young adults, plays a vital role in the economy (Ghana Statistical Service, 2014), with activities like biomass burning contributing to aerosol levels. Additionally, urban areas in Ghana are the major hub for economic activities and substantial emissions from industries, transportation, construction, petroleum extraction, and mining, further impacting aerosol concentrations (Fosu-Amankwah et al., 2021). This study aims to explore these aerosol dynamics in Ghana's evolving environmental landscape, offering valuable insights for scientific research. Despite the multitude of potential aerosol emission sources, systematic assessment of aerosols in Ghana is notably lacking in the existing scientific literature. Hence the need to assess ML performance in forecasting AOD levels with readily available data for our region. The current study therefore aims to provide: i) Spatio-temporal aerosol assessment from MODIS 3km AOD Aqua and Terra products over Ghana; ii) train ML models with meteorological variables; iii) Assess the performance and accuracy of the machine learning model in predicting AOD at different spatial and temporal scales.

2. Dataset and Methodology

2.1. Study Area

The study was carried out in Ghana, situated on the West African Guinea Coast. Ghana experiences a monsoonal climate, characterized by two distinct seasons, dry and wet, due to its tropical location (Aryee et al., 2018). The West African Monsoon (WAM) significantly influences rainfall in the region, along with various convective activities triggered by the movements of the Inter-Tropical Discontinuity (ITD), resulting in a mean annual rainfall ranging from 150 to 2500 mm. It is a component of the global monsoon system, and the shift in the trade wind path in the lower troposphere during the WAM has traditionally been linked to the thermal contrast between the cooler tropical Atlantic and the warmer North African continent (Sultan and Janicot, 2003; Janicot et al., 2011; Louvet et al., 2005). The primary driving forces behind

these wind systems are the energy and temperature differentials between the Gulf of Guinea and the Sahara. Along the ITD, the moist maritime tropical air mass originating from the Atlantic Ocean converges with the dry northeast continental tropical air mass (Amekudzi et al., 2015). The seasonal movement of the ITD gives rise to a bi-modal rainfall pattern in the southern part of Ghana and a uni-modal pattern in the northern region (Owusu and Waylen, 2013). The onset of the rainy season occurs when the maritime tropical air mass is significantly laden with water vapor, typically between the second and third decades of March, with peak precipitation recorded in June. The minor season, lasting only a few weeks, initiates in the first and second decades of September and concludes in the second to third decades of November (Amekudzi et al., 2015; Manzanas et al., 2014). The country experiences an annual average rainfall ranging between 900 and 1900 mm (Baidu et al., 2017). The annual average relative humidity (RH) varies from 77 percent to 85 percent (Williams et al., 2017; Asante and Amuakwa-Mensah, 2014; Kabo-Bah et al., 2016). Ghana is notably one of the fastest-developing countries on the African continent (Amoatey et al., 2018). The nation boasts four key urban centers: Accra, Kumasi, Takoradi, and Tamale. However, this rapid economic growth coupled with population growth, industrialization, and a surge in vehicular density seems to have contributed to incremental growth in air pollution in the country, particularly in these urban centers. Furthermore, findings from Agyemang-Bonsu et al. (2010) indicate that a considerable number of vehicles imported into Ghana are aging, receive limited maintenance, and consequently contribute to elevated emission levels. As of September 2018, over 28,000 deaths in Ghana were linked to air pollution (World Health Organisation, 2016; Odonkor et al., 2020). The World Health Organization (WHO) reported that Ghana's annual average PM2.5 level in 2016 was 31.1 $\mu g/m^3$, well above the recommended guideline of $10\mu g/m^3$ (World Health Organisation, 2016).

2.2. Dataset

2.2.1. MODIS

MODIS serves as the pivotal instrument aboard NASA's Terra and Aqua satellites, launched in December 1999 and May 2002, respectively. Terra follows an orbit from north to south across the equator in the morning, whereas Aqua's orbit goes from south to north over the equator in the afternoon. With Terra MODIS and Aqua MODIS working in tandem, they achieve a comprehensive view of the Earth's surface approximately every one to two days. This remarkable feat is achieved by capturing data across 36 spectral bands, spanning wavelengths from 0.4 to 14.385 μm. The visual richness of MODIS imagery emerges with spatial resolutions of 250m, 500m, and 1km (Kahn et al., 2009; Zhang and Reid, 2009; Shi et al., 2015; Acharya

and Sreekesh, 2013). Of noteworthy significance are the specific channels with wavelengths spanning from 0.47 to 2.12μm, adeptly employed for retrieving vital aerosol characteristics. In further detail, this instrumental suite produces daily-level aerosol optical thickness data, expertly mapped at a global spatial resolution of 10 km $\times$ 10 km. The MODIS swath width is 2330 km, slightly narrower than that of AVHRR. As a result, the coverage for a single day is not complete, and any gaps from one day are filled in on the next. For an animation illustrating the MODIS scan pattern, refer to `http://aqua.nasa.gov/sites/default/files/aqua_modis_h264.mov` (last accessed: 27 July 2023). The retrieval of aerosol data through MODIS employs three distinct algorithms, each designed for specific settings: DT and DB algorithms are employed over land, while the DT algorithm is used over oceans (Hsu et al., 2019). Additionally, the DTB algorithm harmonizes these main approaches, selecting the most suitable one based on the land's characteristics. The DT algorithm is tailored for dark surfaces like dark soil and vegetation. Meanwhile, the advanced second-generation DB algorithm is adept at bright surfaces such as deserts, urban areas, and vegetated regions. The retrieval process of aerosol properties using the DT algorithm over dense vegetation and dark soil relies on how visible wavelengths, specifically 0.47 and 0.65 μm, correlate with a shortwave of 2.12 μm in the infra-red range (Levy et al., 2007). The present operational MODIS dataset, denoted as C061, furnishes standard aerosol characteristics with a spatial resolution of 10 $\times$ 10 km^2 within the Level 2 (L2) datasets, specifically MOD04 for Terra and MYD04 for Aqua. In aggregated Level 3 (L3) products, this resolution is lowered to 1° $\times$ 1°. Furthermore, an additional aerosol file based on the Dark Target (DT) approach with a resolution of 3 km is included in the C006 dataset, which has been continued in the current C061. This enhancement serves to offer air quality insights at local or urban scales. Detailed information about the C006 dataset is elaborated by (Remer et al., 2013), while the progression from the DT C006 to the current C061 is detailed from (Mattoo, 2017). It is noteworthy that the DT product may exhibit relatively higher uncertainty, particularly when applied to bright underlying surfaces (Levy et al., 2010). The monthly AOD dataset at a wavelength of $\lambda = 0.55$ μm for Terra at 10:30 am local time and for Aqua at 1:30 pm local time during overpass times was downloaded from `https://ladsweb.modaps.eosdis.nasa.gov/forthestudy` (last accessed on 27 July 2023).

2.2.2. Input Variables

To predict the AOD from MODIS, climate variables such as temperature(t2m; K), dew-point(K), surface net downward shortwave flux(Jm^{-2}), surface upward longwave flux (Jm^{-2}), surface upward latent heat flux (Jm^{-2}), relative humidity, boundary layer height(m), Down-

ward UV radiation (Jm^{-2}), Evaporation (m), Precipitation(m), Pressure (hPa), Top net solar radiation (Jm^{-2}), and low cloud cover. We utilized these covariates, primarily relying on expert knowledge and data availability. Meteorological variables are known for their influence on the dispersion and transport of fine particulate matter. Atmospheric heat flux variables are also known to be influenced by aerosols which can lead to negative or positive radiative forcing. As previously mentioned, AOD is a key predictor of $PM_{2.5}$, with higher levels of AOD indicating higher $PM_{2.5}$ levels (Wang et al., 2003; Liu et al., 2007; Van Donkelaar et al., 2006, 2010; Gupta et al., 2006). In general, the MinMaxScaler normalizer and the normalization layer from Keras tensorflow were used to normalize and standardize the input data. All climate variables used in prediction were obtained from ERA5 (`https://cds.climate.copernicus.eu/`) with a temporal range spanning 2003 to 2019. A total of 80% of the data was used for training and 20% was used for testing. The DT and deep blue DB combined products were used for this study. The decision to use this product was mainly due to the highly variable topography of our region. Here, we incorporate meteorological data to predict AOD levels, from 1st January 2003 to 31st December 2019 over the entire country and some selected locales.
Table 1 represents the statistical distribution of the input variables for the model.

Table 1: Descriptive Statistics of Covariates Used.

Variables	Count	Mean	Standard Deviation	Minimum	25%	50%	75%	Maximum
t2m	204	303.02	1.73	299.75	301.30	303.296	304.38	307.33
d2m	204	295.24	2.087	281.60	294.92	295.79	296.40	297.54
RH	204	62.28	8.97	27.45	56.89	64.79	69.63	73.60
SH	204	-164.16	62.11	-342.88	-212.80	-136.27	-112.29	-81.22
LH	204	-230.03	48.33	-353.90	-263.17	-228.46	-193.69	-78.18
DS	204	542.92	95.05	333.19	456.26	558.37	616.44	745.10
UL	204	-63.65	22.82	-140.17	-76.46	-56.27	-46.11	-34.08
BLH	204	597.63	109.32	410.93	514.22	579.73	673.09	940.14
AQUA	204	0.47	0.27	0.15	0.28	0.39	0.55	1.50
TERRA	204	0.53	0.26	0.16	0.34	0.46	0.61	1.62

2.2.3. Data Preprocessing

The issue of missing (NaN) values is a prominent challenge commonly faced in the analysis of satellite-borne data products. In this study, we employed a methodology outlined by Fosu-Amankwah et al. (2021) to ensure a cohesive analysis of Aerosol Optical Depth (AOD) datasets. This involved partitioning the country into smaller grids ($0.04^\circ \times 0.04^\circ$) and employing an averaging technique on pixel values (a minimum of three) within these grids to address missing data instances. The practice of averaging data within reduced grids is a conventional approach

in spatial analysis, particularly in the context of remote sensing data and other geospatial datasets characterized by substantial missing or NaN values. In this research, the entire country and specific major localities were considered, with AOD datasets from AQUA and TERRA serving as dependent variables, while other satellite-borne data products, including temperature, dewpoint, surface upward longwave flux, surface upward latent heat flux, surface net downward shortwave flux, relative humidity, boundary layer height, Downward UV radiation, Evaporation, Precipitation, Pressure, Top net solar radiation, and low cloud cover, constituted the independent variables. Given the inherent variation in spatial resolution among the diverse data products utilized in this study, all data products not conforming to the 1 km $\times$ 1 km grid were standardized through bilinear interpolation. The bilinear interpolation method was chosen primarily for its versatility, as it strikes a balance between computational efficiency and accuracy (Arif and Akbar, 2005). This makes it suitable for a broad spectrum of applications where smooth interpolation between gridded data points is essential. Additionally, the temporal resolution of independent variables was adjusted to align with AOD datasets from Aqua and Terra, ensuring consistency.

2.3. Model Development

While performing the data preprocessing, it became evident that the MODIS dataset contained a substantial number of missing values (NaN), which further compounded the scarcity of ground-level observations for $PM_{2.5}$. To bridge this disparity, the integration of various machine learning algorithms emerged as a requisite approach to facilitate the comprehensive evaluation, continuous monitoring, and precise forecasting of Aerosol Optical Depth (AOD) values. These prognostic outcomes have multifaceted utility, including but not limited to data imputation, model parameterization, and broader assessments about regional air quality. One of the main goals of this study was to use ML to assess Aerosol Optical Depth (AOD) in certain areas of Ghana. As the no free lunch (NFL) theorem states; there is no single algorithm that performs best for all possible problems. Hence, we employed two well-known machine learning methods that are often used to predict AOD based on previous research.

2.3.1. Multiple Linear Regression(MLR)

The MLR model is a well-known ML algorithm utilized in establishing the linear relationships among numerous independent variables and a continuous dependent variable. Prior to constructing the MLR model, an extensive review of existing literature was undertaken to assimilate and implement the most effective methodologies outlined in prior research studies. Notably, the MLR model, unlike certain other machine learning algorithms, does not involve

a lot of hyperparameter tuning. However, akin to various machine learning techniques, proper normalization of covariates holds paramount importance in ensuring optimal model performance. Consequently, the MinMaxScaler normalizer was employed in this study to standardize our covariates. This choice was motivated by the method's widespread adoption in numerous studies, predominantly due to its efficiency and computational expediency, making it a popular choice in the scientific community. The mathematical representation of the MLR model is given in equation 1 as:

$$y = \beta_0 + \beta_1 x_1 + \beta_2 x_2 + \ldots + \beta_p x_p + \epsilon \tag{1}$$

where:

$$y : \text{Dependent variable}$$
$$x_1, x_2, \ldots, x_p : \text{Independent variables}$$
$$\beta_0, \beta_1, \beta_2, \ldots, \beta_p : \text{Regression coefficients}$$
$$\epsilon : \text{Error term}$$

2.3.2. Multi Linear Regression(MLR) Using ANN

Before constructing the neural network using the optimal parameters determined through the hyperparameter tuning process, we employed the Artificial Neural Network (ANN) model for conducting a multi-linear regression analysis. This was executed by defining a single input layer and an output layer while excluding any hidden layers during model construction. The fundamental principle of linear regression is to capture linear associations between the dependent variable and independent variables. By structuring the ANN model with solely an input and output layer, it effectively operates akin to a linear regression model. This is mainly because one of the fundamental differences between a linear regression model and a neural network, even with just input and output layers, is the activation function. Linear regression models directly output a weighted sum of inputs without applying any non-linear transformation. In contrast, neural networks typically use activation functions, even in the hidden layers, to introduce non-linearity. This non-linearity allows neural networks to discern complex patterns and relationships in the data. For this model, the Adam optimizer was utilized with a specific learning rate set at 0.01. A batch size of 12 and a total of 89 epochs were employed during the training process. It is noteworthy that these hyperparameters were tuned using the trial-and-error approach.

2.3.3. Artificial Neural Network(ANN)

ANNs are computational models inspired by the intricate neural networks in living organisms. They are renowned for their adept utilization of the backpropagation error technique, a pivotal method for training these networks. This technique revolves around iteratively fine-tuning the network's weights to minimize the discrepancy between anticipated and actual outputs. This intricate process encompasses several essential steps. In the forward pass, input data traverses through the network layer by layer. Neurons calculate weighted sums of inputs, subsequently processed by activation functions to yield neuron outputs. The distinction between predicted and target outputs is computed via a designated error or loss function, like the Mean Squared Error (MSE) for regression or Cross-Entropy for classification. Calculated derivatives guide the adjustment of weights and biases within the network using optimization algorithms, often Gradient Descent or its variants. This endeavor strives to discern weight adjustments that curtail the error. The iterative repetition of this process over multiple epochs refines weights, progressively diminishing errors. Convergence towards an optimal weight configuration, minimizing the error function, characterizes the network's learning trajectory. Influential hyperparameters like activation functions and learning rates can be selected through manual methods, involving trial and error, or alternative strategies such as grid search, random search, or Bayesian optimization. In this study, grid search was employed to identify optimal parameters, as detailed in Table 2. The training of the model involved the application of the Adam optimizer, primarily chosen mainly due to its fast convergence. Additionally, the MSE was employed as the loss function during the training process. The mathematical representation of the MLPN is given in equation 2 as:

$$y_j = f\left(\sum_{i=1}^{N} x_{ji} \cdot w_{ji} + b_j\right) \tag{2}$$

where:

y_j is the output of node j,

f is the activation function,

x_{ji} represents the input from node i to node j,

w_{ji} denotes the weight associated with the connection between node i and node j,

b_j stands for the bias of node j.

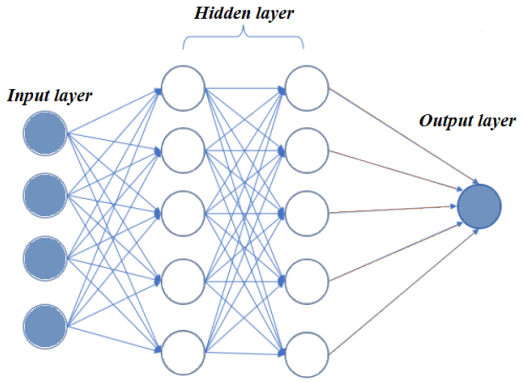

Figure 1: Artificial Neural Network Structure.

Figure 1 depicts the architecture of the ANN model, commonly referred to as the Multilayer Perceptron Network (MLPN). This model falls within the category of Feed-forward backpropagation Neural Networks (FFNN), characterized by its composition of multiple hidden layers and input/output layers that enable the seamless flow of data throughout the network (Bedi et al., 2020).

2.3.4. Hyper-Parameter Tuning

While machine learning methods eliminate the need for certain distribution assumptions, they introduce another factor known as hyper-parameters, which essentially act as guiding settings during the learning process. To fine-tune these hyper-parameters, we conducted a grid search, evaluating model performance based on mean square error and cross-validation R^2 values (indicating prediction accuracy). For our neural network component, we took further steps to enhance its performance. Specifically, we optimized the architecture by selecting three hidden layers and adjusting the number of neurons within them. Moreover, we made necessary refinements such as determining the optimal number of learning iterations (epochs), choosing an appropriate activation function for the neurons, the batch size, dropout rate and fine-tuning the speed at which the model adapts its learning rate. All of these measures were implemented to yield the most effective outcomes from our model. This whole tuning process was done using Keras tuner. Table 2 depicts the result of the tuning process.

Table 2: Best hyperparameters from Keras tuner.

Hidden Layer	Neurons	Learning Rate	Activation Function	Dropout Rate	Batch size
1	71	0.001	ReLU	0.2	16
2	65	0.001	ReLU	0.2	16
3	10	0.001	ReLU	0.2	16

2.4. Validation Metrics

The control parameters of the models were initially chosen and then adjusted through trials to achieve the most optimal fitness measures. To assess the effectiveness of the proposed models, four statistical indicators were employed: root mean square error (RMSE), coefficient of determination (R^2), mean absolute error (MAE), and the Kling-Gupta Efficiency (KGE).

2.4.1. RMSE

RMSE quantifies the standard deviation of the disparities between predicted and observed values, known as residuals. A diminished RMSE signifies a model with reduced errors. The formula for RMSE is depicted in equation 3 as:

$$RMSE = \sqrt{\frac{1}{n}\sum_{i=1}^{n}(\text{pred}_i - \text{observed}_i)^2} \tag{3}$$

2.4.2. MAE

The MAE signifies the average of the absolute differences between the predicted and observed values in the dataset. A smaller MAE value indicates a more accurate model, as it reflects reduced errors. The formula for MAE is depicted in equation 4 as:

$$MAE = \frac{1}{n}\sum_{i=1}^{n}|\text{observed}_i - \text{pred}_i| \tag{4}$$

2.4.3. R^2

The R^2 indicates the fraction of the variance in the dependent variable that can be predicted by the independent variables in the model. It ranges from 0 to 1, where 1 indicates a perfect fit. A higher R-squared value suggests that the model explains a larger portion of the variability in the data. The formula for R^2 is depicted in equation 5 as:

$$R^2 = 1 - \frac{\sum_{i=1}^{n}(\text{observed}_i - \text{pred}_i)^2}{\sum_{i=1}^{n}(\text{observed}_i - \text{mean of observed})^2} \tag{5}$$

2.4.4. KGE

The KGE is a metric used to evaluate model performance. It combines correlation, mean ratio, and variability ratio. A perfect match between observed and simulated data yields a KGE value of 1, indicating optimal model performance. The formula for KGE is depicted in equation 6 as:

$$\text{KGE} = 1 - \sqrt{(r-1)^2 + (\beta-1)^2 + (\gamma-1)^2} \tag{6}$$

Where:

- r is the correlation coefficient between observed and predicted values,
- β is the ratio of the standard deviation of predicted values to the standard deviation of observed values,
- γ is the ratio of the mean of predicted values to the mean of observed values.

3. Results and Discussion

3.1. AOD distribution over Ghana

The representation of aerosol levels across Ghana's climatology is depicted in Figures 2a and 2b. These visuals are derived from AOD measurements at a wavelength of 550 nm, collected over sixteen years (2003-2019) using MODIS. Figures 2a and 2b showcase the geographical distribution of AOD values across the nation, providing a clear demonstration of MODIS's effectiveness in capturing AOD throughout Ghana. The average AOD values for Aqua and Terra over Ghana were 0.470 ($\pm$ 0.206 sd) and 0.528 ($\pm$ 0.208 sd), respectively. When compared to its Aqua equivalent, the Terra DTB algorithm produced results with higher mean AOD. Discrepancies in aerosol statistics between Terra and Aqua, despite their shared data processing techniques, can be attributed to disparities in their orbital characteristics and the timing of satellite overpasses. Terra follows a descending orbital trajectory, traversing the equator in a southward direction around 10:30 am local solar time. Conversely, Aqua ascends northward and undertakes its data collection roughly at 1:30 pm local time. The relatively short temporal interval of approximately 3 hours between the overpasses of the Aqua and Terra satellites offers a unique opportunity to merge data from both sources. This collaborative approach holds the potential to mitigate data losses, primarily attributed to cloud-related issues. These variations in overpass timings, shaped by the distinct orbital trajectories of the satellites, introduce the potential for disparate aerosol statistics to emerge. These differences may arise due to the influence of diurnal aerosol or cloud cycles, contributing to distinct sampling outcomes (Levy et al., 2018). Additionally, the Terra satellite, with its morning overpass, is more inclined to encounter aerosols characterized by notable hygroscopic growth during its observational journey. This phenomenon can be attributed to the heightened humidity levels typically prevalent in tropical regions during the morning hours (Moradi et al., 2016). Several studies (Tsai et al., 2011; Wang et al., 2010; Zhang et al., 2016; Engel-Cox et al., 2006) have highlighted the significant influence of ambient RH on the correlation between satellite AOD and PM. Furthermore,

the Terra satellite's morning orbit provides an opportunity to intercept a dense aerosol air mass generated during the morning "rush hour" period. This air mass includes emissions such as soot from wood fires, frequently used for domestic and commercial food preparation in the region, as well as exhaust emissions from older vehicles. These aerosol particles may have been retained within the stable nighttime and morning atmospheric conditions (Fosu-Amankwah et al., 2021). The difference we observed in Aqua and Terra AOD retrievals in our study was approximately 6%. This difference, although noteworthy, contrasts the findings of Levy et al. (2018) and Fosu-Amankwah et al. (2021), who independently reported a more substantial statistical difference of around 13% in global Aqua and Terra AOD retrievals. It is important to highlight that the discrepancy we observed, which is nearly half of their reported difference, may be linked to the fact that we integrated the DTB comprising the DT and DB products, as opposed to their utilization of stand-alone products. Our observations reveal a concentration of elevated AODs in the southwestern region of the country, while sporadically elevated AOD fluctuations manifest along the mid and southeastern boundaries. These findings align with findings from Aklesso et al. (2018) and Fosu-Amankwah et al. (2021). Aklesso et al. (2018) attributed their findings to the geographical characteristics of the southernmost regions of southern West Africa. They pointed out that these areas are predominantly characterized by low elevations. They observed that the multi-year averaged AOD550 (AOD at 550 nm) over this region exhibits an upward trend as the elevation decreases. This phenomenon can be explained by the influence of high terrain, which can either impede or modify wind directions. Such alterations in wind patterns disrupt the horizontal dispersion of pollutants (Ma et al., 2016; Ning et al., 2018), consequently leading to the diminishing in pollutant concentration levels. Furthermore, Fosu-Amankwah et al. (2021) provided additional insights into the factors influencing the elevated AOD values observed in southwestern Ghana. These heightened AOD values are postulated to arise from various sources, including the presence of sea salt spray suspended within the atmospheric column and aerosols originating from specific source regions. These components not only directly contribute to localized dust accumulations but also exert a significant influence on overall aerosol loadings. In contrast, the comparatively higher AODs detected in the middle and eastern sectors of Ghana are likely linked to anthropogenic activities. These activities encompass emissions of both fine and coarse PM, primarily associated with surface mining operations. Furthermore, these elevated AOD levels may result from emissions of BC originating from biomass combustion and aerosols transported from distant source regions. The complex interplay of these factors, coupled with the unique regional topography, contributes to the observed AOD patterns. Of particular note is the presence of the Akuapim-Togo mountain

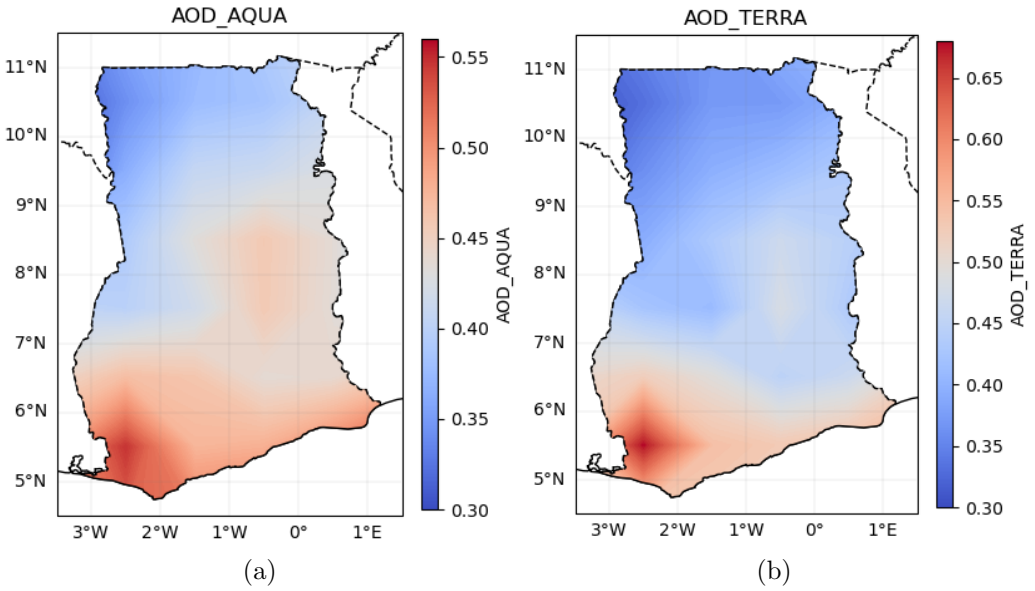

(a) (b)

Figure 2: Average AOD distribution over Ghana for Aqua (a) and Terra (b) retrievals resolution over Ghana spanning 2003-2019

range within the eastern corridors of Ghana. This geographical feature significantly influences the dispersion and containment of aerosols within the region. Consequently, the topographical characteristics of the elevated terrain likely play a crucial role in contributing to the relatively higher AOD levels observed in the eastern sector of the country. These observations underscore the intricate interrelationships between geographical features, human activities, and aerosol dynamics in shaping regional aerosol distribution patterns.

3.2. Feature Importance

According to Mayer and Gróf (2021) and Markovics and Mayer (2022), the process of feature selection stands out as a crucial phase in machine learning, possibly even more important than the model selection itself. Understanding the individual contribution of each covariate to the model's performance is indispensable. The inclusion of irrelevant variables and highly correlated variables, often referred to as multi-collinearity, can significantly impair a model's effectiveness. In this study, we employed both correlation analysis and the intrinsic feature importance attribute derived from the random forest (RF) algorithm. These methods were instrumental in our quest to identify the most optimal features for our models. Figure 3 provides a comprehensive visualization of the contributions made by various covariates for both the AQUA and TERRA datasets, obtained through the RF feature importance property. For TERRA, the most influential feature was the downward shortwave flux, contributing approximately 50%, followed by the latent heat flux, which accounted for around 12% of the variance. Notably, the other features contributed less than 10% individually. Conversely, in the case of AQUA, the

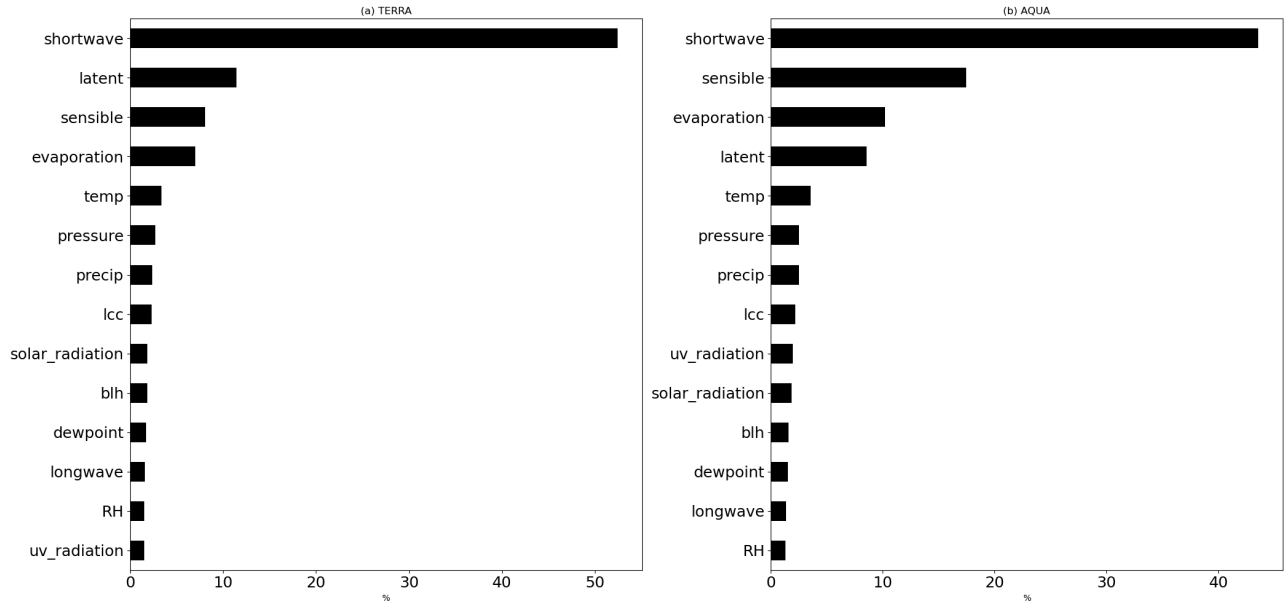

Figure 3: Relative contribution (%) of individual covariates on model performance.

downward shortwave flux remained paramount, contributing about 45%. Here, the influence of latent heat flux decreased significantly, from 12% to 8%. Intriguingly, the contribution of sensible heat flux rose notably from 8% to 17%, making it the second most influential feature for predicting AQUA. The shift between sensible and latent heat flux concerning AQUA and TERRA can be ascribed to the variance in satellite overpass times. For TERRA, the overpass transpires in the morning when the sun has yet to reach its zenith. Overnight, surface temperatures tend to decrease, causing any moisture present on surfaces to undergo a phase change, releasing latent heat. This latent heat energy profoundly influences the aerosols detected by the satellite during its morning overpass. Conversely, AQUA's overpass occurs in the afternoon when the sun shines brightly. By this time, the sun has sufficiently warmed the surface, causing the adjacent air to heat up. Consequently, this warm air ascends, carrying heat energy with it, thereby influencing the aerosols detected by the satellite. Figure 4 illustrates the correlation matrix, a fundamental analytical tool employed in this study. The correlation matrix serves a dual purpose: firstly, it aids in identifying covariates that exhibit strong correlations with the target variable. Secondly, it facilitates the detection of variables displaying high intercorrelations, thereby assisting in mitigating the challenge of multicollinearity. Through the elimination of highly correlated and redundant variables, the selected set comprises the following key parameters: downward shortwave flux, latent heat flux, sensible heat flux, evaporation, pressure, and temperature.

3.3. Spatial Patterns of the Predicted AOD Levels

To evaluate the models' predictive abilities of the spatiotemporal distribution of AOD at a 1km resolution over the region, an array of validation and performance metrics were employed, as previously detailed in section 2.4. Machine learning models were applied across the entirety of the region. Figures 5a and 5b illustrate the diverse metrics utilized for evaluating the predictive capabilities of TERRA and AQUA data, respectively. In Fig 5a, the first row showcases RMSE values. Minimal RMSE values were observed for nearly the entire country, particularly in the northern and middle sectors, ranging from 0.025 to 0.100. Notably, all models exhibited suboptimal performance in the southwestern sector of the country, with RMSE values nearing 0.200. Similarly, the second row, representing Mean Absolute Error (MAE) values, displayed a comparable bias. Models performed exceptionally well in the northern and middle sectors, exhibiting MAE values ranging from 0.100 to 0.175. Conversely, in the southwestern part of the country, all models demonstrated elevated MAE values, approaching 0.300. Moreover, the third row, which depicts the R^2, both MLR and ANN(MLR) models surpassed the traditional ANN model with hidden layers, yielding R^2 values ranging from 0.50 to 0.85 across the entire country. Notably, in the southwestern part of the country, both the traditional ANN and ANN(MLR) models outperformed the MLR model. Finally, the last row illustrates KGE values for the models. It is evident from the figure that both the traditional ANN and ANN(MLR) models outperformed the MLR model, specifically in the middle and southern sectors of the country, where KGE values ranged from 0.50 to 0.8. Notably, the MLR model exhibited comparatively low KGE values in the southwestern part of the country compared to the other models.

In Fig. 5b, the first row depicts RMSE values for various models' predictions of AOD from the AQUA satellite across the study area. Among these models, the ANN(MLR) model demonstrated exceptional performance, displaying RMSE values ranging from 0.025 to 0.125 nationwide. Conversely, both the traditional ANN and MLR models exhibited comparatively inferior performance, specifically in the middle and southern sectors of the country, where RMSE values ranged from 0.125 to 0.175. In the second row, denoting MAE, all models performed remarkably well in the northwestern part of the country, displaying MAE values ranging from 0.125 to 0.200. In the middle and southern sectors, ANN demonstrated superior performance, closely followed by ANN(MLR). MLR, however, displayed the lowest performance in these sectors, with values ranging from 0.225 to 0.300. Moving to the third row representing the R^2, the MLR model exhibited superior performance nationwide, closely followed by ANN(MLR). The traditional ANN model showcased notable proficiency, particularly in the northwestern and eastern parts of the middle sector, where R^2 values ranged from 0.5 to 0.75. Conversely,

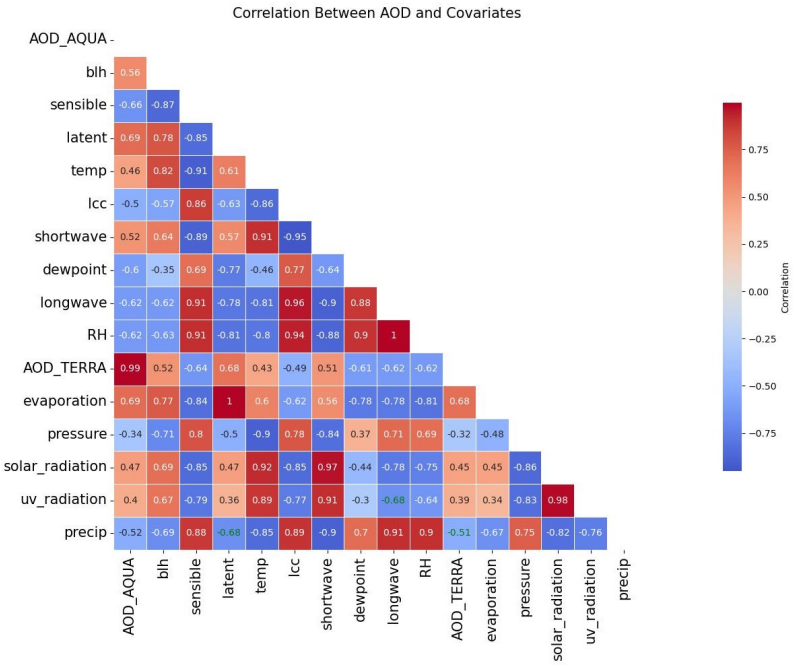

Figure 4: Correlation Matrix.

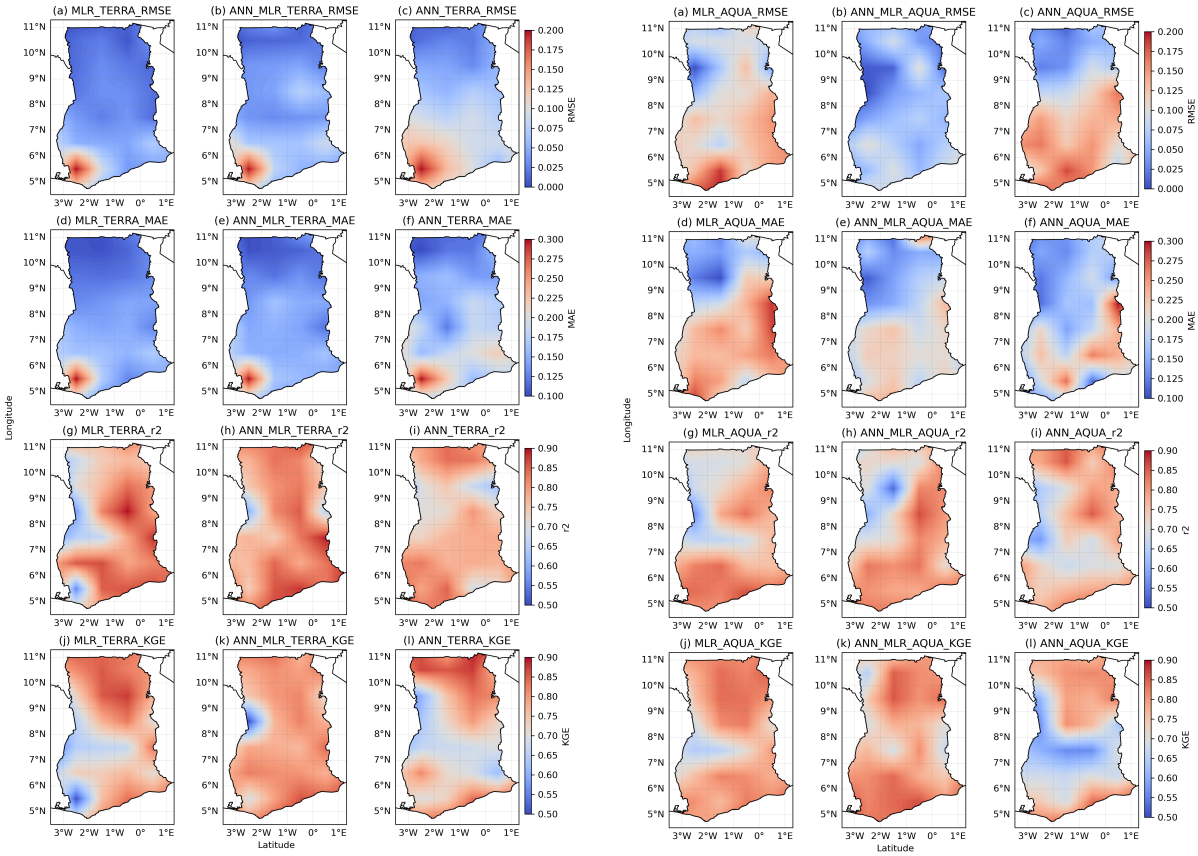

(a) (b)

Figure 5: Error Metrics for the Predicted Spatial Distribution of AOD levels for Terra (a) and Aqua (b) retrievals over Ghana spanning 2003-2019

in the western part of the middle sector extending towards the southern region, both MLR and ANN(MLR) models displayed superior performance. In the final row, representing KGE values, all models demonstrated high KGE values, especially in the northern and southern sectors, ranging from 0.50 to 0.85. However, within the middle sector, the ANN(MLR) model displayed superior performance, closely followed by the traditional ANN model. MLR yielded lower KGE values in this sector, ranging from 0.1 to 0.25.

On average, the models demonstrated exceptional predictive accuracy for AQUA and TERRA data across much of the country, particularly in the northern and middle regions. However, challenges arose in the southern sector, particularly in the southwestern and specific middle regions. This difficulty can be attributed to the exclusive utilization of meteorological variables as input data in our models. The southwestern region, as detailed by Fosu-Amankwah et al. (2021), is characterized by substantial vegetation cover. Under low to moderate temperatures, dense vegetation could potentially serve as a significant source of biogenic aerosols, as noted by Charlson et al. (1992). Consequently, this phenomenon could influence aerosol optical depths, especially observed by TERRA during its morning overpass. Additionally, the presence of dense vegetation in the area could lead to challenges related to illegal timber cutting which occurs mostly during nighttime, directly contributing to local dust loadings and plant debris. These factors, in turn, impact aerosol loading. Unfortunately, the absence of readily available ground observation data prevented the incorporation of such meaningful covariates into our models. Consequently, our models were limited in their ability to efficiently learn from these complex environmental variables, underscoring the importance of integrating comprehensive datasets for more accurate and nuanced predictions.

3.4. ML aerosol assessments over selected locales.

Within the framework of our machine learning evaluations, our attention was directed toward Accra and Takoradi, two significant urban hubs within Ghana's landscape. Accra, being the nation's capital, boasts a substantial population of approximately 3 million (Rain et al., 2011; Ghana Statistical Service, 2019). Its demographic expansion is notably rapid, given its status as a primary recipient of migrants compared to other regions (Ghana Statistical Service, 2019). In contrast, Takoradi, often referred to as the oil city, is a coastal metropolitan area situated about 280 km west of Accra, positioned within the southwestern expanse of Ghana. Upon analyzing the AOD datasets across major Ghanaian cities, our analysis revealed that these two metropolitan regions exhibited the highest mean aerosol burden. Specifically, Accra demonstrated readings of 0.56 for TERRA and 0.48 for AQUA, while Takoradi displayed values

of 0.56 for TERRA and 0.51 for AQUA. The escalated aerosol levels in Accra can be attributed to rapidly increasing population figures, extensive industrial and economic activities, and a high volume of vehicular traffic, especially during morning rush hours, leading to significant vehicular emissions. Conversely, in Takoradi, heightened aerosol burdens could result from emissions originating from offshore oil rigs and gas industries. The transport of these emissions over the city is influenced by factors such as wind direction, speed, and proximity to the coastline. This influential observation enabled our research focus: to assess the predictive capabilities of the employed machine learning models in simulating and predicting fluctuations in aerosol burden levels within these locales. Our objective was to critically evaluate the performance of these models under such critical circumstances. Figure 6 presents a comparative analysis of observed and simulated AOD levels over Accra and Takoradi, employing machine learning models developed within this study.

In the case of Accra (AQUA) represented in the first row, the ANN(MLR) model demonstrated superior performance, exhibiting an RMSE value of 0.18, MAE value of 0.203, R^2 value of 0.75, and a KGE value of 0.72. Following closely was the MLR model, outperforming the ANN model. Notably, the ANN model displayed noteworthy skill in terms of MAE values, boasting the lowest MAE value of 0.163. Refer to Table 3 for a comprehensive summary of the utilized metrics. In the context of Accra (TERRA), all models demonstrated commendable performance. However, considering KGE values, ANN(MLR) surpassed both the MLR and ANN models. Notably, the MLR model exhibited the lowest KGE value at 0.45, compared to the impressive 0.72 for ANN(MLR) and 0.69 for ANN. Moving to Takoradi (AQUA), the ANN(MLR) model exhibited exceptional proficiency, yielding an RMSE value of 0.110, MAE value of 0.122, R^2 value of 0.72, and the highest recorded KGE value among the models at 0.76. Subsequently, the MLR model and the ANN model followed suit. Finally, examining Takoradi (TERRA) in the last row, all models showcased commendable performance in simulating AOD levels over the region. Yet, the ANN(MLR) model demonstrated superior accuracy, closely trailed by the MLR model and then the ANN model. Specifically, the ANN(MLR) model displayed an RMSE value of 0.173, MAE value of 0.273, R^2 value of 0.67, and a KGE value of 0.63. Notably, the MLR model recorded the lowest KGE value, standing at 0.31. A detailed summary of the various metrics employed in this analysis is presented in Table 3.

4. Conclusions

The study delineates a comprehensive spatio-temporal assessment of aerosol distribution across Ghana and two of its prominent cities using MODIS AOD data at a spatial resolution of

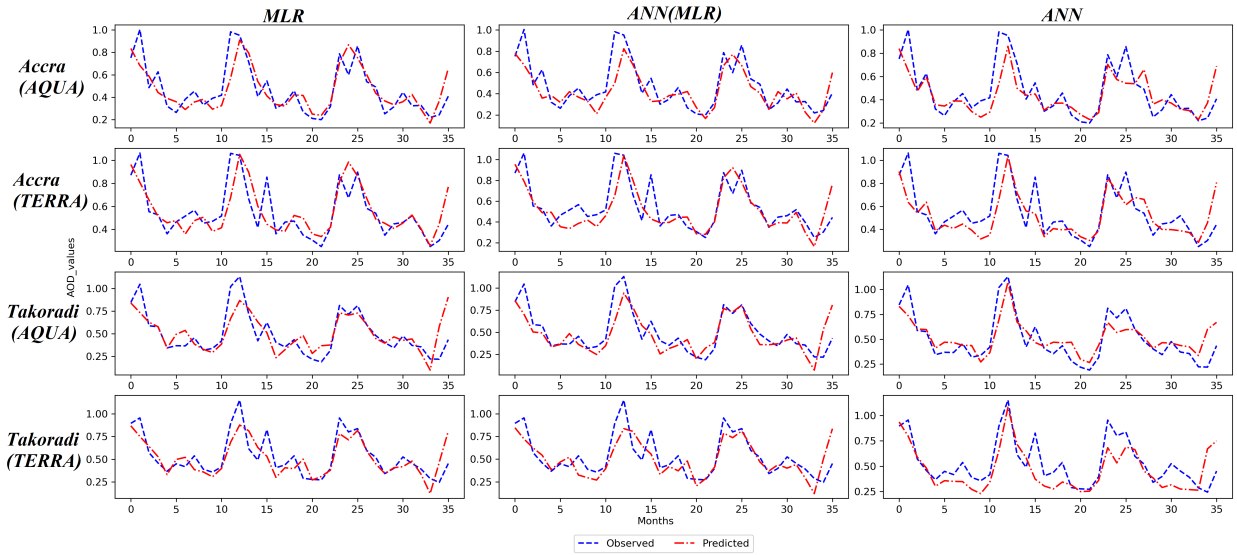

Figure 6: Comparison between predicted and observed variations in AOD levels over selected locales.

Table 3: Summary of the Various Metrics employed over selected locales

		Results		
Location	Metrics	MLR	ANN(MLR)	ANN
Accra(AQUA)	RMSE	0.12	0.08	0.12
	MAE	0.23	0.20	0.16
	R^2	0.73	0.75	0.43
	KGE	0.69	0.72	0.67
Accra(TERRA)	RMSE	0.08	0.09	0.10
	MAE	0.18	0.18	0.19
	R^2	0.76	0.72	0.21
	KGE	0.45	0.72	0.69
Tarkoradi(AQUA)	RMSE	0.18	0.11	0.17
	MAE	0.24	0.12	0.21
	R^2	0.74	0.72	0.25
	KGE	0.61	0.76	0.67
Tarkoradi(TERRA)	RMSE	0.19	0.17	0.19
	MAE	0.28	0.27	0.27
	R^2	0.21	0.67	0.24
	KGE	0.31	0.63	0.60

1 km. This investigation spans a sixteen-year period (2003–2019) and delves into the intricate patterns of aerosol distribution and concentration. AOD is a key predictor of $PM_{2.5}$, with higher levels of AOD indicating higher $PM_{2.5}$ levels, a relationship underscored by several referenced studies.

Guided by the principle of the No Free Lunch (NFL) theorem, which underscores the absence of a universally optimal algorithm for all problems, we undertook an evaluation of the performance of two distinct machine learning algorithms in predicting AOD values over the entire country and some selected locales, specifically, Accra and Takoradi. The selection of these regions is grounded in their status as major cities in Ghana, characterized by the highest mean aerosol burden in comparison to other significant urban centers. To the best of our knowledge, this study is the first to use machine learning models to perform AOD assessments over the country. The following conclusions are drawn:

1. The analysis of spatio-temporal aerosol distribution revealed noteworthy insights. The examination of MODIS Aqua and Terra AOD retrievals unveiled an overall lower aerosol burden over Ghana, marked by mean AOD values hovering around 0.35. Moreover, the retrieval patterns demonstrated a subtle variance of approximately 0.06 between the mean Terra and Aqua AODs. Our research reveals distinctive patterns in aerosol concentration across various regions within our study area. The southwestern part of the country consistently exhibits elevated aerosol loadings, while the northern, eastern coastal areas and some parts of the middle sector, consistently display lower aerosol concentrations. This recurring observation aligns with prior studies undertaken in the same geographical vicinity (Aklesso et al., 2018; Fosu-Amankwah et al., 2021) and can be ascribed to various factors. The presence of dense vegetation in the southwestern region likely contributes to this aerosol distribution pattern, possibly linked to increased biogenic emissions. Additionally, Fosu-Amankwah et al. (2021) suggested that elevated aerosol loadings in the southwestern sector of the country result from a combination of factors, including the complex dynamics of sea salt spray deposition from oceanic bubble eruptions and emissions from the petroleum and gas sectors along the western coast. The proximity of these coastal phenomena to the southwestern region significantly contributes to higher aerosol concentrations. Aklesso et al. (2018) also attributed their findings to geographical characteristics in southern West Africa, where low elevations prevail and elevated terrain can alter wind patterns, affecting pollutant dispersion.
2. Utilizing a comprehensive range of validation metrics for assessing model performance, we

can confidently conclude all models developed in the study exhibited an acceptable level of accuracy. However, the MLR Regression utilizing the ANN architecture ANN(MLR), exhibited superior predictive capabilities compared to both the original MLR and the standard Keras-tuned ANN model.

3. The sub-optimal performance of the standard ANN model aligns with previous research (He et al., 2016; Srivastava and Singh, 2015), indicating that standard feed-forward neural networks might encounter issues related to saturation and reduced accuracy as the number of hidden layers increases, as observed in various similar studies. This modest performance of the ANN model might be attributed to inherent limitations. Specifically, two prominent limitations include overfitting, where the model becomes too closely tailored to training data, leading to poorer generalization on unseen data, and the requirement of substantial data, which often necessitates large datasets to achieve meaningful learning. Other noteworthy limitations include the local minimum trap and the exploding gradient problems. More information on these limitations can be found in (Shang and Wah, 1996).
4. In the selected major cities, the presence of elevated pollution levels, predominantly attributed to biogenic and anthropogenic emissions, is a defining characteristic. However, our analysis of MODIS data preprocessing revealed a widespread occurrence of NaN (Not a Number) values. This challenge, coupled with limited ground-level observations, severely constrains our ability to systematically monitor and forecast air quality in these urban centers and the broader region. Leveraging machine learning models presents a promising solution to mitigate this substantial constraint. These models offer an effective approach for monitoring and predicting air quality using readily accessible data sources, while maintaining an acceptable level of accuracy, thereby overcoming the limitations posed by data gaps and enabling more robust environmental assessments.
5. For future studies, it's worth noting that the datasets we used in our research have a relatively basic level of detail in terms of spatial resolution. To improve the precision of upcoming studies, it would be beneficial to consider datasets from other data sources with finer spatial resolutions. These more detailed datasets would allow for quicker and more thorough assessments of aerosol distributions and related factors, providing a more comprehensive understanding of the subject matter. Also, our analysis primarily concentrated on meteorological variables as input data for the models. However, it is recommended that future investigations consider the integration of additional variables, such as land use characteristics, population growth patterns, vehicular emissions, agricultural residue burning, domestic waste burning, industrial/biogenic emissions, the density of transporta-

tion hubs, and daily traffic counts. These supplementary variables can provide a more holistic understanding of the factors influencing aerosol distribution and facilitate more comprehensive predictive models.

Declaration of competing interest

The authors declare that they have no known competing financial interests or personal relationships that could have appeared to influence the work reported in this paper.

Funding

This research received no external funding

References

Abokyi, E., Appiah-Konadu, P., Abokyi, F., and Oteng-Abayie, E. F. (2019). Industrial growth and emissions of co2 in ghana: the role of financial development and fossil fuel consumption. *Energy Reports*, 5:1339–1353.

Acharya, P. and Sreekesh, S. (2013). Seasonal variability in aerosol optical depth over india: a spatio-temporal analysis using the modis aerosol product. *International journal of remote sensing*, 34(13):4832–4849.

Agyemang-Bonsu, K., Dontwi, I., Tutu-Benefoh, D. a., Bentil, D., Boateng, O., Asuobonteng, K., and Agyemang, W. (2010). Traffic-data driven modelling of vehicular emissions using copert iii in ghana: A case study of kumasi.

Aklesso, M., Kumar, K. R., Bu, L., and Boiyo, R. (2018). Analysis of spatial-temporal heterogeneity in remotely sensed aerosol properties observed during 2005–2015 over three countries along the gulf of guinea coast in southern west africa. *Atmospheric Environment*, 182:313–324.

Amekudzi, L. K., Yamba, E. I., Preko, K., Asare, E. O., Aryee, J., Baidu, M., and Codjoe, S. N. (2015). Variabilities in rainfall onset, cessation and length of rainy season for the various agro-ecological zones of ghana. *Climate*, 3(2):416–434.

Amoatey, P., Omidvarborna, H., and Baawain, M. (2018). The modeling and health risk assessment of pm2. 5 from tema oil refinery. *Human and Ecological Risk Assessment: An International Journal*, 24(5):1181–1196.

Apte, J. S., Marshall, J. D., Cohen, A. J., and Brauer, M. (2015). Addressing global mortality from ambient pm2. 5. *Environmental science & technology*, 49(13):8057–8066.

Arif, F. and Akbar, M. (2005). Resampling air borne sensed data using bilinear interpolation algorithm. In *IEEE International Conference on Mechatronics, 2005. ICM'05.*, pages 62–65. IEEE.

Aryee, J., Amekudzi, L., Quansah, E., Klutse, N., Atiah, W., and Yorke, C. (2018). Development of high spatial resolution rainfall data for ghana. *International Journal of Climatology*, 38(3):1201–1215.

Asante, F. A. and Amuakwa-Mensah, F. (2014). Climate change and variability in ghana: Stocktaking. *Climate*, 3(1):78–101.

Bai, Y., Zeng, B., Li, C., and Zhang, J. (2019). An ensemble long short-term memory neural network for hourly pm2. 5 concentration forecasting. *Chemosphere*, 222:286–294.

Baidu, M., Amekudzi, L. K., Aryee, J. N., and Annor, T. (2017). Assessment of long-term spatio-temporal rainfall variability over ghana using wavelet analysis. *Climate*, 5(2):30.

Bedi, S., Samal, A., Ray, C., and Snow, D. (2020). Comparative evaluation of machine learning models for groundwater quality assessment. *Environmental Monitoring and Assessment*, 192:1–23.

Boucher, O., Randall, D., Artaxo, P., Bretherton, C., Feingold, G., Forster, P., Kerminen, V.-M., Kondo, Y., Liao, H., Lohmann, U., et al. (2013). Clouds and aerosols. In *Climate change 2013: The physical science basis. Contribution of working group I to the fifth assessment report of the intergovernmental panel on climate change*, pages 571–657. Cambridge University Press.

Cai, S., Wang, Y., Zhao, B., Wang, S., Chang, X., and Hao, J. (2017). The impact of the "air pollution prevention and control action plan" on pm2. 5 concentrations in jing-jin-ji region during 2012–2020. *Science of the Total Environment*, 580:197–209.

Charlson, R. J., Schwartz, S., Hales, J., Cess, R. D., Coakley Jr, J., Hansen, J., and Hofmann, D. (1992). Climate forcing by anthropogenic aerosols. *Science*, 255(5043):423–430.

Chu, D., Kaufman, Y., Ichoku, C., Remer, L., Tanré, D., and Holben, B. (2002). Validation of modis aerosol optical depth retrieval over land. *Geophysical research letters*, 29(12):MOD2–1.

Chu, D. A., Kaufman, Y., Zibordi, G., Chern, J., Mao, J., Li, C., and Holben, B. (2003). Global monitoring of air pollution over land from the earth observing system-terra moderate resolution imaging spectroradiometer (modis). *Journal of Geophysical Research: Atmospheres*, 108(D21).

Creamean, J. M., Suski, K. J., Rosenfeld, D., Cazorla, A., DeMott, P. J., Sullivan, R. C., White, A. B., Ralph, F. M., Minnis, P., Comstock, J. M., et al. (2013). Dust and biological aerosols from the sahara and asia influence precipitation in the western us. *science*, 339(6127):1572–1578.

Dabass, A., Talbott, E. O., Rager, J. R., Marsh, G. M., Venkat, A., Holguin, F., and Sharma, R. K. (2018). Systemic inflammatory markers associated with cardiovascular disease and acute and chronic exposure to fine particulate matter air pollution (pm2. 5) among us nhanes adults with metabolic syndrome. *Environmental research*, 161:485–491.

Dandou, A., Bosioli, E., Tombrou, M., Sifakis, N., Paronis, D., Soulakellis, N., and Sarigiannis, D. (2002). The importance of mixing height in characterising pollution levels from aerosol optical thickness derived by satellite. *Water, Air and Soil Pollution: Focus*, 2:17–28.

Danesh Yazdi, M., Kuang, Z., Dimakopoulou, K., Barratt, B., Suel, E., Amini, H., Lyapustin, A., Katsouyanni, K., and Schwartz, J. (2020). Predicting fine particulate matter (pm2. 5) in the greater london area: An ensemble approach using machine learning methods. *Remote Sensing*, 12(6):914.

David, L. M., Ravishankara, A., Kodros, J. K., Pierce, J. R., Venkataraman, C., and Sadavarte, P. (2019). Premature mortality due to pm2. 5 over india: Effect of atmospheric transport and anthropogenic emissions. *GeoHealth*, 3(1):2–10.

De Longueville, F., Hountondji, Y.-C., Henry, S., and Ozer, P. (2010). What do we know about effects of desert dust on air quality and human health in west africa compared to other regions? *Science of the total environment*, 409(1):1–8.

Di, Q., Koutrakis, P., and Schwartz, J. (2016). A hybrid prediction model for pm2. 5 mass and components using a chemical transport model and land use regression. *Atmospheric environment*, 131:390–399.

Engel-Cox, J. A., Hoff, R. M., Rogers, R., Dimmick, F., Rush, A. C., Szykman, J. J., Al-Saadi, J., Chu, D. A., and Zell, E. R. (2006). Integrating lidar and satellite optical depth with am-

bient monitoring for 3-dimensional particulate characterization. *Atmospheric Environment*, 40(40):8056–8067.

Engel-Cox, J. A., Holloman, C. H., Coutant, B. W., and Hoff, R. M. (2004). Qualitative and quantitative evaluation of modis satellite sensor data for regional and urban scale air quality. *Atmospheric environment*, 38(16):2495–2509.

Fosu-Amankwah, K., Bessardon, G. E., Quansah, E., Amekudzi, L. K., Brooks, B. J., and Damoah, R. (2021). Assessment of aerosol burden over ghana. *Scientific African*, 14:e00971.

García-Pando, C. P., Stanton, M. C., Diggle, P. J., Trzaska, S., Miller, R. L., Perlwitz, J. P., Baldasano, J. M., Cuevas, E., Ceccato, P., Yaka, P., et al. (2014). Soil dust aerosols and wind as predictors of seasonal meningitis incidence in niger. *Environmental health perspectives*, 122(7):679–686.

Geng, G., Zhang, Q., Martin, R. V., van Donkelaar, A., Huo, H., Che, H., Lin, J., and He, K. (2015). Estimating long-term pm2. 5 concentrations in china using satellite-based aerosol optical depth and a chemical transport model. *Remote sensing of Environment*, 166:262–270.

Ghana Statistical Service (2014). Ghana Statistical Service. `https://www.statsghana.gov.gh`. Accessed: October 27, 2023.

Ghana Statistical Service (2019). Ghana Statistical Service. `https://www.statsghana.gov.gh`. Accessed: October 27, 2023.

Gupta, P., Christopher, S. A., Box, M. A., and Box, G. P. (2007). Multi year satellite remote sensing of particulate matter air quality over sydney, australia. *International Journal of Remote Sensing*, 28(20):4483–4498.

Gupta, P., Christopher, S. A., Wang, J., Gehrig, R., Lee, Y., and Kumar, N. (2006). Satellite remote sensing of particulate matter and air quality assessment over global cities. *Atmospheric Environment*, 40(30):5880–5892.

He, J., Yu, Y., Xie, Y., Mao, H., Wu, L., Liu, N., and Zhao, S. (2016). Numerical model-based artificial neural network model and its application for quantifying impact factors of urban air quality. *Water, Air, & Soil Pollution*, 227:1–16.

Hinds, W. C. and Zhu, Y. (2022). *Aerosol technology: properties, behavior, and measurement of airborne particles*. John Wiley & Sons.

Hsu, N., Lee, J., Sayer, A., Kim, W., Bettenhausen, C., and Tsay, S.-C. (2019). Viirs deep blue aerosol products over land: Extending the eos long-term aerosol data records. *Journal of Geophysical Research: Atmospheres*, 124(7):4026–4053.

Hu, X., Waller, L. A., Al-Hamdan, M. Z., Crosson, W. L., Estes Jr, M. G., Estes, S. M., Quattrochi, D. A., Sarnat, J. A., and Liu, Y. (2013). Estimating ground-level pm2. 5 concentrations in the southeastern us using geographically weighted regression. *Environmental research*, 121:1–10.

Janicot, S., Caniaux, G., Chauvin, F., de Coëtlogon, G., Fontaine, B., Hall, N., Kiladis, G., Lafore, J.-P., Lavaysse, C., Lavender, S. L., et al. (2011). Intraseasonal variability of the west african monsoon. *Atmospheric Science Letters*, 12(1):58–66.

Johnson, B., Shine, K., and Forster, P. (2004). The semi-direct aerosol effect: Impact of absorbing aerosols on marine stratocumulus. *Quarterly Journal of the Royal Meteorological Society*, 130(599):1407–1422.

Jung, C.-R., Young, L.-H., Hsu, H.-T., Lin, M.-Y., Chen, Y.-C., Hwang, B.-F., and Tsai, P.-J. (2017). Pm2. 5 components and outpatient visits for asthma: A time-stratified case-crossover study in a suburban area. *Environmental Pollution*, 231:1085–1092.

Kabo-Bah, A. T., Diji, C. J., Nokoe, K., Mulugetta, Y., Obeng-Ofori, D., and Akpoti, K. (2016). Multiyear rainfall and temperature trends in the volta river basin and their potential impact on hydropower generation in ghana. *Climate*, 4(4):49.

Kahn, R. A. and Gaitley, B. J. (2015). An analysis of global aerosol type as retrieved by misr. *Journal of Geophysical Research: Atmospheres*, 120(9):4248–4281.

Kahn, R. A., Nelson, D. L., Garay, M. J., Levy, R. C., Bull, M. A., Diner, D. J., Martonchik, J. V., Paradise, S. R., Hansen, E. G., and Remer, L. A. (2009). Misr aerosol product attributes and statistical comparisons with modis. *IEEE Transactions on Geoscience and Remote Sensing*, 47(12):4095–4114.

Kanabkaew, T. (2013). Prediction of hourly particulate matter concentrations in chiangmai, thailand using modis aerosol optical depth and ground-based meteorological data. *EnvironmentAsia*, 6(2).

Kato, Y. (2018). Application of dust and pm2. 5 detection methods using modis data to the asian dust events which aggravated respiratory symptoms in western japan in may 2011.

In *Remote Sensing of the Atmosphere, Clouds, and Precipitation VII*, volume 10776, pages 144–159. SPIE.

Kloog, I., Nordio, F., Coull, B. A., and Schwartz, J. (2012). Incorporating local land use regression and satellite aerosol optical depth in a hybrid model of spatiotemporal pm2. 5 exposures in the mid-atlantic states. *Environmental science & technology*, 46(21):11913–11921.

Kondratyev, K. Y., Ivlev, L. S., Krapivin, V. F., and Varostos, C. A. (2006). *Atmospheric aerosol properties: formation, processes and impacts*. Springer Science & Business Media.

Lee, H., Liu, Y., Coull, B., Schwartz, J., and Koutrakis, P. (2011). A novel calibration approach of modis aod data to predict pm 2.5 concentrations. *Atmospheric Chemistry and Physics*, 11(15):7991–8002.

Levy, R., Mattoo, S., Munchak, L., Remer, L., Sayer, A., Patadia, F., and Hsu, N. (2013). The collection 6 modis aerosol products over land and ocean. *Atmospheric Measurement Techniques*, 6(11):2989–3034.

Levy, R., Remer, L., Kleidman, R., Mattoo, S., Ichoku, C., Kahn, R., and Eck, T. (2010). Global evaluation of the collection 5 modis dark-target aerosol products over land. *Atmospheric Chemistry and Physics*, 10(21):10399–10420.

Levy, R. C., Mattoo, S., Sawyer, V., Shi, Y., Colarco, P. R., Lyapustin, A. I., Wang, Y., and Remer, L. A. (2018). Exploring systematic offsets between aerosol products from the two modis sensors. *Atmospheric Measurement Techniques*, 11(7):4073–4092.

Levy, R. C., Remer, L. A., Mattoo, S., Vermote, E. F., and Kaufman, Y. J. (2007). Second-generation operational algorithm: Retrieval of aerosol properties over land from inversion of moderate resolution imaging spectroradiometer spectral reflectance. *Journal of Geophysical Research: Atmospheres*, 112(D13).

Li, L. (2020). A robust deep learning approach for spatiotemporal estimation of satellite aod and pm2. 5. *Remote Sensing*, 12(2):264.

Liu, Y., Franklin, M., Kahn, R., and Koutrakis, P. (2007). Using aerosol optical thickness to predict ground-level pm2. 5 concentrations in the st. louis area: A comparison between misr and modis. *Remote sensing of Environment*, 107(1-2):33–44.

Lohmann, U. and Feichter, J. (2005). Global indirect aerosol effects: a review. *Atmospheric Chemistry and Physics*, 5(3):715–737.

Louvet, S., Fontaine, B., and Roucou, P. (2005). Active phase and pauses of the west african monsoon and associated atmospheric dynamics. In *European Geoscience Union (EGU)*.

Ma, Z., Hu, X., Sayer, A. M., Levy, R., Zhang, Q., Xue, Y., Tong, S., Bi, J., Huang, L., and Liu, Y. (2016). Satellite-based spatiotemporal trends in pm2. 5 concentrations: China, 2004–2013. *Environmental health perspectives*, 124(2):184–192.

Manzanas, R., Amekudzi, L., Preko, K., Herrera, S., and Gutiérrez, J. M. (2014). Precipitation variability and trends in ghana: An intercomparison of observational and reanalysis products. *Climatic change*, 124:805–819.

Markovics, D. and Mayer, M. J. (2022). Comparison of machine learning methods for photovoltaic power forecasting based on numerical weather prediction. *Renewable and Sustainable Energy Reviews*, 161:112364.

Mattoo, S. (2017). Aerosol dark target (10 km & 3 km) collection 6.1 changes.

Mayer, M. J. and Gróf, G. (2021). Extensive comparison of physical models for photovoltaic power forecasting. *Applied Energy*, 283:116239.

Mhawish, A., Banerjee, T., Broday, D. M., Misra, A., and Tripathi, S. N. (2017). Evaluation of modis collection 6 aerosol retrieval algorithms over indo-gangetic plain: Implications of aerosols types and mass loading. *Remote sensing of environment*, 201:297–313.

Ministry of Transport (2016). Ministry of Transport. `https://wedocs.unep.org`. Accessed: November 29, 2023.

Misra, A. K. (2014). Climate change and challenges of water and food security. *International Journal of Sustainable Built Environment*, 3(1):153–165.

Moore, D., Jerrett, M., Mack, W., and Künzli, N. (2007). A land use regression model for predicting ambient fine particulate matter across los angeles, ca. *Journal of Environmental Monitoring*, 9(3):246–252.

Moradi, I., Arkin, P., Ferraro, R., Eriksson, P., and Fetzer, E. (2016). Diurnal variation of tropospheric relative humidity in tropical regions. *Atmospheric Chemistry and Physics*, 16(11):6913–6929.

Nabavi, S. O., Haimberger, L., and Abbasi, E. (2019). Assessing pm2. 5 concentrations in tehran, iran, from space using maiac, deep blue, and dark target aod and machine learning algorithms. *Atmospheric Pollution Research*, 10(3):889–903.

Ning, G., Wang, S., Ma, M., Ni, C., Shang, Z., Wang, J., and Li, J. (2018). Characteristics of air pollution in different zones of sichuan basin, china. *Science of the Total Environment*, 612:975–984.

Odonkor, S. T., Mahami, T., et al. (2020). Knowledge, attitudes, and perceptions of air pollution in accra, ghana: a critical survey. *Journal of environmental and public health*, 2020.

Owusu, K. and Waylen, P. R. (2013). The changing rainy season climatology of mid-ghana. *Theoretical and applied climatology*, 112:419–430.

Prieto-Parra, L., Yohannessen, K., Brea, C., Vidal, D., Ubilla, C. A., and Ruiz-Rudolph, P. (2017). Air pollution, pm2. 5 composition, source factors, and respiratory symptoms in asthmatic and nonasthmatic children in santiago, chile. *Environment international*, 101:190–200.

Putaud, J.-P., Van Dingenen, R., Alastuey, A., Bauer, H., Birmili, W., Cyrys, J., Flentje, H., Fuzzi, S., Gehrig, R., Hansson, H., Harrison, R., Herrmann, H., Hitzenberger, R., Hüglin, C., Jones, A., Kasper-Giebl, A., Kiss, G., Kousa, A., Kuhlbusch, T., Löschau, G., Maenhaut, W., Molnar, A., Moreno, T., Pekkanen, J., Perrino, C., Pitz, M., Puxbaum, H., Querol, X., Rodriguez, S., Salma, I., Schwarz, J., Smolik, J., Schneider, J., Spindler, G., ten Brink, H., Tursic, J., Viana, M., Wiedensohler, A., and Raes, F. (2010a). A european aerosol phenomenology – 3: Physical and chemical characteristics of particulate matter from 60 rural, urban, and kerbside sites across europe. *Atmospheric Environment*, 44(10):1308–1320.

Putaud, J.-P., Van Dingenen, R., Alastuey, A., Bauer, H., Birmili, W., Cyrys, J., Flentje, H., Fuzzi, S., Gehrig, R., Hansson, H.-C., et al. (2010b). A european aerosol phenomenology–3: Physical and chemical characteristics of particulate matter from 60 rural, urban, and kerbside sites across europe. *Atmospheric Environment*, 44(10):1308–1320.

Rain, D., Engstrom, R., Ludlow, C., and Antos, S. (2011). Accra ghana: A city vulnerable to flooding and drought-induced migration. *Case study prepared for cities and climate Change: Global Report on Human Settlements*, 2011:1–21.

Reeves, C., Formenti, P., Afif, C., Ancellet, G., Attié, J.-L., Bechara, J., Borbon, A., Cairo, F., Coe, H., Crumeyrolle, S., et al. (2010). Chemical and aerosol characterisation of the troposphere over west africa during the monsoon period as part of amma. *Atmospheric Chemistry and Physics*, 10(16):7575–7601.

Remer, L., Mattoo, S., Levy, R., and Munchak, L. (2013). Modis 3 km aerosol product: algorithm and global perspective. *Atmospheric Measurement Techniques*, 6(7):1829–1844.

Shang, Y. and Wah, B. W. (1996). Global optimization for neural network training. *Computer*, 29(3):45–54.

Shen, X., Bilal, M., Qiu, Z., Sun, D., Wang, S., and Zhu, W. (2018). Validation of modis c6 dark target aerosol products at 3 km and 10 km spatial resolutions over the china seas and the eastern indian ocean. *Remote Sensing*, 10(4):573.

Shi, K., Zhang, Y., Zhu, G., Liu, X., Zhou, Y., Xu, H., Qin, B., Liu, G., and Li, Y. (2015). Long-term remote monitoring of total suspended matter concentration in lake taihu using 250 m modis-aqua data. *Remote Sensing of Environment*, 164:43–56.

SIERRA-VARGAS, M. P. and Teran, L. M. (2012). Air pollution: Impact and prevention. *Respirology*, 17(7):1031–1038.

Srivastava, D. and Singh, R. M. (2015). Groundwater system modeling for simultaneous identification of pollution sources and parameters with uncertainty characterization. *Water resources management*, 29:4607–4627.

Stafoggia, M., Zauli-Sajani, S., Pey, J., Samoli, E., Alessandrini, E., Basagaña, X., Cernigliaro, A., Chiusolo, M., Demaria, M., Díaz, J., et al. (2016). Desert dust outbreaks in southern europe: contribution to daily pm10 concentrations and short-term associations with mortality and hospital admissions. *Environmental health perspectives*, 124(4):413–419.

Sultan, B. and Janicot, S. (2003). The west african monsoon dynamics. part ii: The "preonset" and "onset" of the summer monsoon. *Journal of climate*, 16(21):3407–3427.

Sunnu, A., Afeti, G., and Resch, F. (2008). A long-term experimental study of the saharan dust presence in west africa. *Atmospheric Research*, 87(1):13–26.

Taghavi-Shahri, S. M., Fassò, A., Mahaki, B., and Amini, H. (2020). Concurrent spatiotemporal daily land use regression modeling and missing data imputation of fine particulate

matter using distributed space-time expectation maximization. *Atmospheric environment*, 224:117202.

Taheri Shahraiyni, H. and Sodoudi, S. (2016). Statistical modeling approaches for pm10 prediction in urban areas; a review of 21st-century studies. *Atmosphere*, 7(2):15.

Thaller, E. I., Petronella, S. A., Hochman, D., Howard, S., Chhikara, R. S., and Brooks, E. G. (2008). Moderate increases in ambient pm 2.5 and ozone are associated with lung function decreases in beach lifeguards. *Journal of occupational and environmental medicine*, pages 202–211.

Tsai, T.-C., Jeng, Y.-J., Chu, D. A., Chen, J.-P., and Chang, S.-C. (2011). Analysis of the relationship between modis aerosol optical depth and particulate matter from 2006 to 2008. *Atmospheric Environment*, 45(27):4777–4788.

Van Donkelaar, A., Martin, R. V., Brauer, M., Kahn, R., Levy, R., Verduzco, C., and Villeneuve, P. J. (2010). Global estimates of ambient fine particulate matter concentrations from satellite-based aerosol optical depth: development and application. *Environmental health perspectives*, 118(6):847–855.

Van Donkelaar, A., Martin, R. V., and Park, R. J. (2006). Estimating ground-level pm2. 5 using aerosol optical depth determined from satellite remote sensing. *Journal of Geophysical Research: Atmospheres*, 111(D21).

Vidale, S. and Campana, C. (2018). Ambient air pollution and cardiovascular diseases: From bench to bedside. *European Journal of preventive cardiology*, 25(8):818–825.

Wang, J., Liu, X., Christopher, S. A., Reid, J. S., Reid, E., and Maring, H. (2003). The effects of non-sphericity on geostationary satellite retrievals of dust aerosols. *Geophysical Research Letters*, 30(24).

Wang, Z., Chen, L., Tao, J., Zhang, Y., and Su, L. (2010). Satellite-based estimation of regional particulate matter (pm) in beijing using vertical-and-rh correcting method. *Remote sensing of environment*, 114(1):50–63.

Wei, J., Peng, Y., Guo, J., and Sun, L. (2019). Performance of modis collection 6.1 level 3 aerosol products in spatial-temporal variations over land. *Atmospheric Environment*, 206:30–44.

WHO (2013). Health effects of particulate matter: Policy implications for countries in eastern europe, caucasus and central asia. *World Health Organization*.

Williams, A. P., Abatzoglou, J. T., Gershunov, A., Guzman-Morales, J., Bishop, D. A., Balch, J. K., and Lettenmaier, D. P. (2019). Observed impacts of anthropogenic climate change on wildfire in california. *Earth's Future*, 7(8):892–910.

Williams, P. A., Crespo, O., Atkinson, C. J., and Essegbey, G. O. (2017). Impact of climate variability on pineapple production in ghana. *Agriculture & Food Security*, 6(1):1–14.

World Health Organisation (2016). World Health Statistics 2016. `https://www.who.int`. Accessed: November 29, 2023.

Wu, Y., de Graaf, M., and Menenti, M. (2016). Improved modis dark target aerosol optical depth algorithm over land: Angular effect correction. *Atmospheric Measurement Techniques*, 9(11):5575–5589.

Xiao, F., Yang, M., Fan, H., Fan, G., and Al-Qaness, M. A. (2020). An improved deep learning model for predicting daily pm2. 5 concentration. *Scientific reports*, 10(1):20988.

Xu, J., Jiang, H., Xiao, Z., Wang, B., Wu, J., and Lv, X. (2016). Estimating air particulate matter using modis data and analyzing its spatial and temporal pattern over the yangtze delta region. *Sustainability*, 8(9):932.

Yu, H., Kaufman, Y., Chin, M., Feingold, G., Remer, L., Anderson, T., Balkanski, Y., Bellouin, N., Boucher, O., Christopher, S., et al. (2006). A review of measurement-based assessments of the aerosol direct radiative effect and forcing. *Atmospheric Chemistry and Physics*, 6(3):613–666.

Yung, J. A., Fuseini, H., and Newcomb, D. C. (2018). Hormones, sex, and asthma. *Annals of Allergy, Asthma & Immunology*, 120(5):488–494.

Zeng, X., Xu, X., Zheng, X., Reponen, T., Chen, A., and Huo, X. (2016). Heavy metals in pm2. 5 and in blood, and children's respiratory symptoms and asthma from an e-waste recycling area. *Environmental pollution*, 210:346–353.

Zhang, J. and Reid, J. S. (2009). An analysis of clear sky and contextual biases using an operational over ocean modis aerosol product. *Geophysical Research Letters*, 36(15).

Zhang, T., Gong, W., Zhu, Z., Sun, K., Huang, Y., and Ji, Y. (2016). Semi-physical estimates of national-scale pm10 concentrations in china using a satellite-based geographically weighted regression model. *Atmosphere*, 7(7):88.